Performance and Characterization of Supported Rhenium Oxide Catalysts for Selective Oxidation of Methanol to Methylal

Youzhu Yuan[†] and Yasuhiro Iwasawa*

Department of Chemistry, Graduate School of Science, The University of Tokyo, Hongo, Bunkyo-ku, Tokyo 113-0033, Japan

Received: October 10, 2001; In Final Form: January 4, 2002

The unique performances of supported rhenium oxide catalysts for the selective oxidation of methanol to methylal (dimethoxymethane) [$3CH_3OH + {}^1/_2O_2 \rightarrow CH_2(OCH_3)_2 + 2H_2O$] were examined in a fixed-bed flow reactor and in a pulse reactor. Rhenium oxides supported on α-Fe_2O_3, γ-Fe_2O_3, and V_2O_5 among many oxide supports showed high activities (15−49% conversion) and selectivities (90−94% selectivity) for catalytic methylal synthesis at 513 K. These Re catalysts are the first to show good performances for one-stage methylal synthesis from methanol. The catalysts were characterized by XRD, XPS, TPR, TPD, and FTIR spectroscopy to provide insight into the active Re species relevant to the selective oxidation of methanol to methylal. Rhenium oxides on α-Fe_2O_3 were dispersed as tetrahedral ReO_4 species up to one monolayer at 0.7 wt % Re loading. It was suggested that active Re−Fe−O mixed-oxide clusters were formed above 1 wt % Re. ReO_2 crystallites were also observed for the Re/α-Fe_2O_3 samples with Re loadings above 6 wt %. On γ-Fe_2O_3, which has a higher surface area, no ReO_2 species were observed. It is suggested that the redox capability of rhenium oxides, $Re^{6-7+} \rightleftarrows Re^{4+}$, is responsible for the catalytic performance, although appropriate Lewis acidity of the rhenium oxides is also necessary for the acetalization of formaldehyde with methanol to methylal. The oxide supports prevent rhenium oxides from being sublimated and reduced to ReO_2 particles.

1. Introduction

The ability of rhenium oxides to take a variety of oxidation states that are illustrated in both binary and ternary oxides,[1−5] might allow for the exploitation of new catalytic chemistry and applications. Supported Re catalysts are highly active and selective in metathesis reactions.[6,7] Rhenium is also an important component in a rheniforming catalytic process.[8] Further, sulfided Re catalysts might be more active than conventional Co−Mo−S catalysts in hydrodesulfurization.[9,10] Nevertheless, rhenium oxides have not been employed as a key species in catalytic selective oxidation reactions because of sublimation under reaction conditions.[11]

Few reports have been devoted to this topic, and they have described the failure of the use of inorganic Re compounds for catalytic oxidation.[12] These negative contributions of rhenium oxides to oxidation processes is somewhat surprising because the oxides of tungsten and osmium, which are neighbors of rhenium in the periodic table, work as efficient epoxidation and *cis*-hydroxylation catalysts, respectively.[13−16] It was reported that methyltrioxorhenium (CH_3ReO_3) was active for alkene epoxidation at or below room temperature.[17,18] In contrast to other metal-containing epoxidation catalysts, almost no decomposition of H_2O_2 occurred with CH_3ReO_3. The unique oxidation property of CH_3ReO_3 has generated much interest in high-valence oxo-organometallic chemistry.[19−21]

We have found that crystalline $SbRe_2O_6$ is active for the catalytic selective oxidation of methanol to form methylal (dimethoxymethane), $CH_2(OCH_3)_2$, where three methanol molecules are incorporated into a methyal molecule [$3CH_3OH + {}^1/_2O_2 \rightarrow CH_2(OCH_3)_2 + 2H_2O$].[22,23] The selectivity to methylal reached 92.5% at a conversion of 6.5% at 573 K. Methylal is used as a gasoline additive, a solvent in the perfume industry, a key intermediate for preparing high-concentration formaldehyde, and a reagent in organic syntheses. The activity and selectivity of the $SbRe_2O_6$ catalyst for the methylal synthesis were much higher than those of other catalysts reported to date, such as V/TiO_2,[24] V−Mo−O,[25] PMoH-5.75/SiO_2,[26,27] Mo/MCM-41,[28] MoO_3(100) plane,[29] and so on.[30] Industrially, methylal is produced by two-stage processes: methanol oxidation to formaldehyde on silver and ferric molybdate catalysts and dehydrative condensation of the formaldehyde with methanol with sulfuric acid. Thus, the one-stage heterogeneous reaction process on the $SbRe_2O_6$ catalyst has economical and environmental benefits in the production of methylal. It was suggested that the performance of the crystalline $SbRe_2O_6$ catalyst was due to the rhenium oxide connecting with Sb−O chains. The surface area of the crystalline $SbRe_2O_6$ is as low as 1 $m^2\ g^{-1}$, which might be a disadvantage in applications to catalytic processes.

Recently, we revealed the ability of supported rhenium oxides to selective catalyze the oxidation of methanol to methylal.[31] The present study reports, in detail, the performances of supported rhenium oxide catalysts for the selective oxidation of methanol of methylal, the effects of the support and the Re loading on the performance, and the characterization of the active Re species by XRD, XPS, TPR, TPD, and FTIR spectroscopy.

* To whom correspondence should be addressed. E-mail: iwasawa@chem.s.u-tokyo.ac.jp. Fax: 81-3-5800-6892.

[†] Permanent address: Department of Chemistry, State Key Laboratory for Physical Chemistry of Solid Surface, Xiamen University, Xiamen 361005, China.

10.1021/jp013770l CCC: $22.00
Published on Web 03/21/2002

2. Experimental Section

2.1. Catalyst Preparation. Supported rhenium oxide catalysts were prepared by an incipient wetness impregnation method using an aqueous solution of ammonium perrhenate (NH_4ReO_4; Soekawa Chemical Co., 99.99% purity), followed by evaporation to remove the solvent on a water bath and drying at 383 K for 12 h. Commercially available oxides such as TiO_2 (rutile), TiO_2 (anatase), V_2O_5, ZrO_2, α-Fe_2O_3, γ-Fe_2O_3, SiO_2, α-Al_2O_3, Sb_2O_3, Bi_2O_3, and MoO_3 were used as supports. The Re loadings were varied in the range of 0−10 wt % as Re/support. The samples were put into a glass fixed-bed reactor in a flow system and heated to 673 K at a heating rate of 4 K min^{-1} in a He flow and held at 673 K for 6 h. The samples thus obtained were further treated in situ in the fixed-bed flow reactor under He flow at 573 K for 1 h before use as catalysts. Unsupported rhenium oxides such as ReO_3 (Soekawa) and ReO_2 (Soekawa) were also pretreated at 673 K in a similar way.

2.2. Catalytic Methanol Oxidation. The catalytic reactions on the supported and unsupported rhenium oxide catalysts were carried out in a conventional fixed-bed flow reactor. The catalytic performances were examined in the temperature range 473−553 K under the reaction conditions GHSV = 40 000 mL h^{-1} $g_{cat}{}^{-1}$ and $He/O_2/MeOH$ = 86.3/9.7/4.0 (mol %) at 1 atm. The mixture was regulated by mass flow controllers. Methanol (Wako Chemical Co., purity 99.8%) was introduced into the flow reactor by bubbling He gas through a glass saturator filled with methanol. The outlet stream line from the reactor to a gas chromatograph was heated at about 423 K to avoid condensation of reaction products. The products were analyzed by an on-line gas chromatograph using Porapak N (3 m) and Unibeads (3 m) C columns.

2.3. Catalyst Characterization. Surface areas of the samples were measured by a BET nitrogen adsorption method at 77 K using a BELSORP36 machine.

XRD patterns were measured on a Rigaku Miniflex goniometer. The analysis was carried out in a continuous $\theta/2\theta$ scan reflection mode using Cu Kα radiation (λ = 0.154 18). The anode was operated at 30 kV and 15 mA. The 2θ angles were scanned from 5 to 80° at a rate of 2°/min.

XPS spectra were measured on a Rigaku XPS-7000 spectrometer using Mg Kα radiation (1253.6 eV) with X-ray power of 200 W (accelerating voltage 20 kV, emission current 10 mA). Samples were pressed into thin disks, placed on holders, outgassed to less than 2.6×10^{-5} Pa in a prechamber, and transferred to an analysis chamber. The procedures for sample preparation for the XPS measurement were conducted in a glovebox filled with high-purity N_2 to avoid the samples contact with air as much as possible. The binding energy was referred to 284.6 eV for C 1s. The peak deconvolution and fitting were performed using SpXzeigR2.1 software running with Igor Pro and a Gaussian−Lorentzian line shape, with both the spin−orbit splitting and the relative intensity of the spin−orbit components fixed.

Pyridine TPD spectra were recorded in a flow reactor equipped with an on-line gas chromatograph that was monitored by a GC workstation. The catalyst (200 mg) was pretreated at a given temperature under a He flow (Linder Co., purity 99.995%) for 1 h and then cooled to 298 K under a He flow. Pyridine was introduced into the flow reactor by bubbling He gas through a glass saturator filled with pyridine. Pyridine adsorption was conducted for 30 min at 298 K. The flow involving pyridine was switched to pure He for at least 1 h until a straight GC baseline was obtained. The TPD spectra were recorded at a ramping rate of 10 K min^{-1}. The effluent gas from the reactor was analyzed by an on-line gas chromatograph.

TPR spectra were recorded in the same flow reactor system. The catalyst (30 mg) was pretreated at a given temperature under a He flow for 1 h and then cooled to 298 K under a He flow. The He flow was switched to a 7% H_2/Ar flow, and then TPR measurements were made at a ramping rate of 10 K min^{-1}. The effluent gas from the reactor was analyzed by an on-line gas chromatograph.

FTIR spectra were measured on a Perkin-Elmer Spectrum 2000 instrument with a MCT detector at a resolution of 4 cm^{-1}. ReO_x/α-Fe_2O_3 was pressed into a self-supporting thin disk, which was placed in a quartz IR cell with CaF_2 windows combined in a vacuum system. The sample in the IR cell was heated at a rate of 4 K min^{-1} to 673 K and held at 673 K for 30 min under vacuum. Then, the sample was cooled to 298 K and exposed to dry pyridine (3×10^2 Pa), followed by evacuation at 373 K for 30 min. The FTIR spectra were measured after evacuation at given temperatures from 373 to 623 K and recorded as difference spectra from the spectrum for the sample before pyridine adsorption. For comparison, spectra of the α-Fe_2O_3 support were also measured.

3. Results

3.1. Methanol Oxidation on Supported Re Catalysts. Selective methanol oxidation to methylal on several oxide-supported ReO_x catalysts was performed at 513 K under the reaction conditions of GHSV = 40 000 mL h^{-1} $g_{cat}{}^{-1}$ and $He/O_2/MeOH$ = 86.3/9.7/4.0 (mol %). Table 1 shows the performances of the supported rhenium oxide catalysts, where the 100% conversion of methanol corresponds to a reaction rate of 65.4×10^{-3} mol h^{-1} $g_{cat}{}^{-1}$. The performances of bulk rhenium oxides (ReO_3 and ReO_2) and two typical supports (α-Fe_2O_3 and V_2O_5) are also listed in Table 1 for comparison. It was found that rhenium oxides supported on TiO_2 (rutile and anatase), V_2O_5, ZrO_2 (monoclinic), Fe_2O_3 (α and γ), and α-Al_2O_3 were active in order of the reaction rates per gram of Re for the supports TiO_2(anatase) > TiO_2 (rutile) > γ-Fe_2O_3 > ZrO_2 > V_2O_5 > α-Al_2O_3 ≥ α-Fe_2O_3. Of the samples, Re/V_2O_5, Re/γ-Fe_2O_3, Re/α-Fe_2O_3, Re/ZrO_2, and Re/α-Al_2O_3 showed selectivities of 88−94% to methylal at 513 K. Rhenium oxides supported on SiO_2 produced a significant amount of CO_x (CO_2 and CO), and those supported on Sb_2O_3 and Bi_2O_3 showed no activity at 513 K (Table 1). α-Fe_2O_3 and V_2O_5 themselves were almost inactive for methylal formation, although V_2O_5 produced formaldehyde. When these oxides were supported by rhenium oxides, the obtained Re/α-Fe_2O_3 and Re/V_2O_5 samples showed selectivities to methylal as high as 90.5−93.7% at 513 K. ReO_3 was most selective (99% selectivity), while the selectivity of ReO_2 was lower (64.6% for commercial ReO_2; 84.2% for ReO_2 prepared by decomposition of NH_4ReO_4 at 673 K). When the mixture of $He/MeOH/O_2$ was admitted to Re_2O_7 at 513 K, the color changed from yellow (Re_2O_7) to red (ReO_3) in less than 3 min, accompanied by sublimation of some of the Re_2O_7, and the catalyst showed a selectivity to methylal of >90% after 10 min of time on stream. This indicates that bulk Re_2O_7 is not a stable phase under catalytic reaction conditions.

Plots of selectivity versus conversion per unit surface area for the supported ReO_x catalysts are shown in Figure 1. It was found that Re/α-Fe_2O_3, Re/γ-Fe_2O_3, Re/V_2O_5, and Re/ZrO_2 exhibited high catalytic performances for the selective methylal synthesis. No deactivation of the supported rhenium oxides occurred for 6 h of time on stream at 513 K. There was no significant change in the surface area of the oxide samples with

TABLE 1: Catalytic Methanol Oxidation on Supported Rhenium Oxide Catalysts at 513 K[a]

catalyst	S_{BET} ($m^2\ g^{-1}$)	MeOH conversion mol %	MeOH conversion rate (mmol $h^{-1}\ g_{Re}^{-1}$)	selectivity(mol %) $CH_2(OCH_3)_2$	HCHO	$(CH_3)_2O$	$HCOOCH_3$	CO_x[b]
10 wt % Re/TiO_2−rutile (1)	5	53.7	351.2	83.1	1.9	0.7	9.1	5.2
10 wt % Re/TiO_2−anatase (2)	50	59.5	389.1	78.5	4.1	1.1	11.7	4.6
10 wt % Re/V_2O_5 (3)	6	21.5	140.6	93.7	0.0	4.3	0.0	2.0
10 wt % Re/ZrO_2 (4)	9	35.8	234.1	89.4	2.0	trace	7.6	1.0
10 wt % Re/α-Fe_2O_3 (5)	3	15.5	101.4	90.5	2.0	1.0	6.0	0.5
10 wt % Re/γ-Fe_2O_3 (6)	16	48.4	319.2	91.0	2.4	1.0	4.6	1.0
10 wt % Re/Fe_2O_3[c]	23	51.6	337.5	82.7	2.6	0.6	9.5	4.6
10 wt % Re/SiO_2 (7)	36	15.1	98.8	60.7	1.3	trace	11.9	26.1
10 wt % Re/α-Al_2O_3 (8)	10	16.3	106.6	88.3	2.8	trace	5.9	2.9
10 wt %Re/Sb_2O_3	1	0.0	0.0	0.0	0.0	0.0	0.0	0.0
10 wt % Re/Bi_2O_3	1	0.0	0.0	0.0	0.0	0.0	0.0	0.0
10 wt % Re/MoO_3 (9)	5	9.1	59.5	80.0	0.0	19.0	0.0	1.0
α-Fe_2O_3 (Soekawa)	3	0.0	0.0	0.0	0.0	0.0	0.0	0.0
V_2O_5 (Soekawa)	6	9.3	10.8[d]	1.0	91.5	7.4	0.0	trace
ReO_3 (Soekawa)	1	12.4	10.2	99.0	0.0	0.5	0.5	0.0
ReO_2 (Soekawa)	7	65.3	50.0	64.6	6.4	2.0	10.2	16.8
ReO_x[e]	1	10.0	7.7	84.2	0.0	8.9	5.9	1.0

[a] GHSV = 40 000 mL $h^{-1}\ g_{cat}^{-1}$, $He/O_2/MeOH$ = 86.3/9.7/4.0 (mol %). [b] CO_2 + CO. [c] Fe_2O_3 was prepared by adding an aqueous solution of NH_4OH (Wako, purity 99.9%) to an aqueous solution of $Fe(NO_3)_3$, followed by filtration, washing with deionized water, drying at 393 K, and calcining at 673 K for 4 h in air. [d] Units of mol $h^{-1}\ g_V^{-1}$. [e] ReO_x was obtained by temperature-programmed calcination (4 K/min) of NH_4ReO_4 at 673 K for 6 h in He, and the crystalline phase thus obtained is mainly due to monoclinic ReO_2 by XRD. The numbers in parentheses are used for numbering the supported ReO_x catalysts in Figure 1.

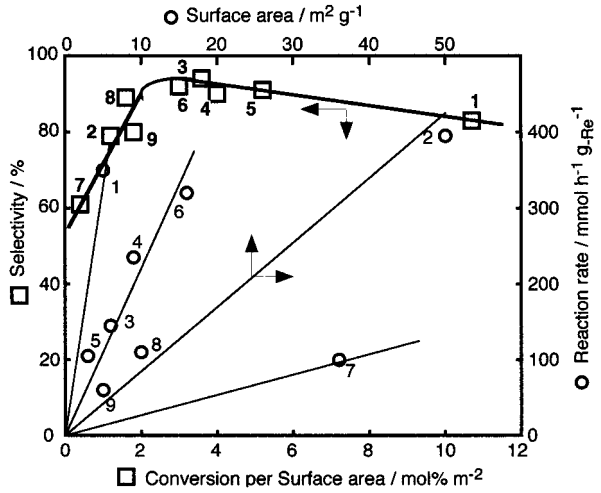

Figure 1. Dependency of the selectivity to methylal on the conversion per unit surface area (□) and dependency of the reaction rate per gram of Re on the surface area (○) of the supported ReO_x catalysts with 10 wt % Re: 1, Re/TiO_2 (rutile); 2, Re/TiO_2 (anatase); 3, Re/V_2O_5; 4, Re/ZrO_2; 5, Re/α-Fe_2O_3; 6, Re/γ-Fe_2O_3; 7, Re/SiO_2; 8, Re/α-Al_2O_3; 9, Re/MoO_3.

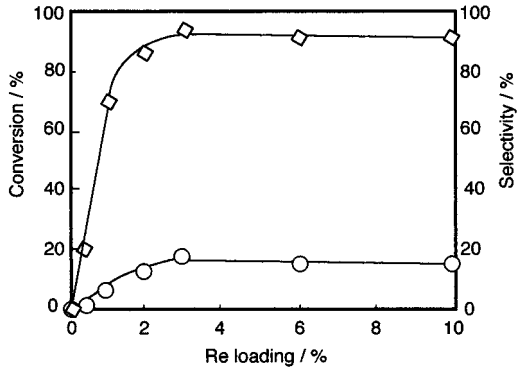

Figure 2. Variations of the conversion and selectivity with Re loading in the Re/α-Fe_2O_3 catalysts. Reaction temperature = 513 K, GHSV = 40 000 mL $h^{-1}\ g_{cat}^{-1}$, $He/O_2/MeOH$ = 86.3/9.7/4.0 (mol %). ○, MeOH conversion; ◇, methylal selectivity.

Re loading. The reaction rates per gram of Re are also plotted versus surface area in Figure 1, which provides information on the efficiency per 1 wt % Re quantity for each catalyst. The reaction rate increased with the surface area, with four straight lines for four oxide groups indicating the different reactivities of the rhenium oxide species. This is consistent with the results of the plots of selectivity vs conversion/surface area. For example, Re/α-Fe_2O_3, Re/V_2O_5, Re/ZrO_2, and Re/γ-Fe_2O_3 are classified in the same group, but Re/TiO_2 (anatase), Re/α-Al_2O_3 and Re/MoO_3 are classified in another group. The rhenium oxide species of the catalysts in the same group are regarded to have similar activities for the catalytic selective oxidation of methanol to methylal.

3.2. Effects of Re Loading and Reaction Temperature. Figure 2 shows the methanol conversion and the selectivity to methylal as a function of Re loading in the Re/α-Fe_2O_3 catalyst. Both methanol conversion and methylal selectivity increased with increasing Re loading and reached maximum values of 18.1 and 93.7%, respectively, at 3 wt % Re. Above this loading the conversion and selectivity decreased slightly to 15.5 and 90.5%, respectively, at 10 wt % Re.

Figure 3 shows the methanol conversion and the selectivities to several products including methylal, formaldehyde, and methylformate as functions of reaction temperature. The methanol conversion increased with increasing temperature, whereas the methylal selectivity passed through a maximum at 513 K and then decreased with increasing temperature. The decrease in selectivity was due to an increase in formaldehyde formation, and the formation of undesired products such as methylformate and CO_x (CO_2 and CO) was still low. These results confirm that supported Re catalysts are promising catalysts for selective methanol oxidation.

3.3. Pulse Reaction. Pulses of ca. 1 mL of a mixture of 96.0/4.0 (mol %) He/MeOH in the absence of O_2 were introduced onto the 10 wt % Re/α-Fe_2O_3 catalyst at 513 K at an interval of about 15 min. Figure 4 presents plots of the methanol conversion and the selectivities to several products versus the number of the methanol pulses. Methylal was formed in the first to fourth methanol pulses, but the selectivity decreased to zero at the fifth pulse. The formation of formaldehyde also

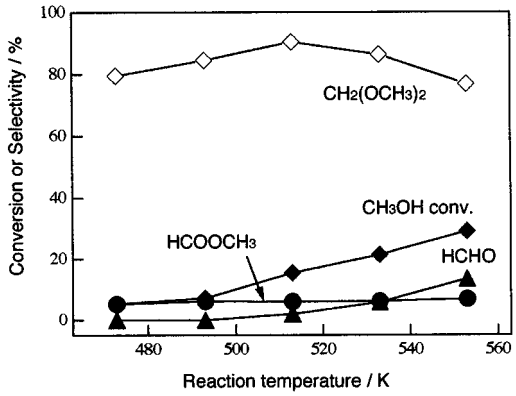

Figure 3. Variations of the conversion and selectivity with reaction temperature in methanol conversion to methylal on the 10 wt % Re/α-Fe_2O_3 catalyst with GHSV = 40 000 mL h^{-1} g_{cat}^{-1} and He/O_2/MeOH = 86.3/9.7/4.0 (mol %). ◆, MeOH conversion; ◇, methylal selectivity; ●, methyl formate selectivity; ▲, formaldehyde selectivity.

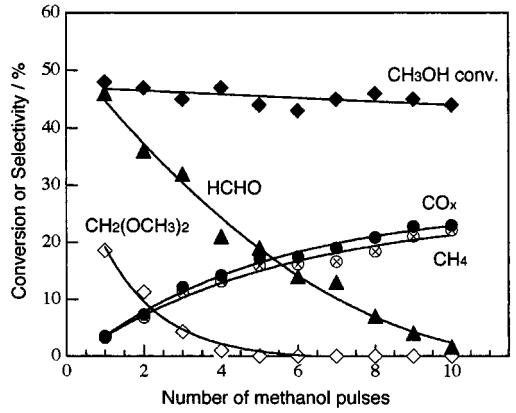

Figure 4. Pulse experiments: conversion and selectivity vs number of methanol pules [He/MeOH = 96/4 (mol %)] on the 10 wt % ReO_x/α-Fe_2O_3 catalyst at 513 K. ◆, MeOH conversion; ◇, methylal selectivity; ▲, formaldehyde selectivity; ●, CO_x selectivity; ⊗, CH_4 selectivity.

decreased but more gently with increasing number of methanol pulses and continued throughout the 10 pulses. Methylal formation might be favorable on the catalyst surfaces with more lattice oxygen as compared to formaldehyde formation. The formation of dimethyl ether (not shown) also decreased with the number of pulses, in agreement with the decrease in methylal formation because both reactions involve intermolecular dehydration processes. Methylformate formation (not shown) decreased with the number of methanol pulses, whereas the formations of H_2, CH_4, and CO_2 increased throughout the 10 pulses. The molecular ratio of H_2, CH_4, and CO_2 was approximately 2:1:1, which agrees with the assumptions that methylformate is produced by a dehydrogenative condensation of formaldehyde with methanol ($CH_3OH \rightarrow HCHO + H_2$, $HCHO + CH_3OH \rightarrow HCOOCH_3 + H_2$) and CH_4 and CO_2 are produced by decomposition of the methylformate ($HCOOCH_3 \rightarrow CH_4 + CO_2$).[23]

3.4. Characterization by XRD and XPS. Figure 5 shows the XRD patterns for various Fe_2O_3-supported ReO_x catalysts, bulk rhenium oxides, and iron oxides. Calcination of NH_4ReO_4 at 673 K in He produced monoclinic crystalline ReO_2 as evidenced by XRD,[32] whereas the 6 wt % Re/α-Fe_2O_3, 10 wt % Re/γ-Fe_2O_3, and 10 wt % Re/Fe_2O_3 [prepared from $Fe(NO_3)_3$] catalysts exhibited no diffraction pattern except for the XRD patterns for the α-Fe_2O_3 or γ-Fe_2O_3 support. The results imply that rhenium oxides are dispersed on the supports without

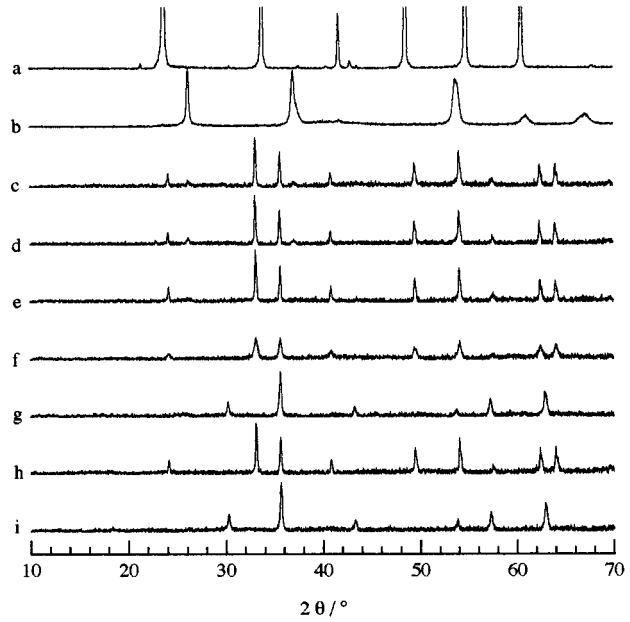

Figure 5. XRD patterns for the Re/α-Fe_2O_3 catalysts: (a) commercially available ReO_3, (b) commercially available ReO_2, (c) 10 wt % Re/α-Fe_2O_3, (d) 10 wt % Re/α-Fe_2O_3 after methanol oxidation at 513 K for 2 h, (e) 6 wt % Re/α-Fe_2O_3, (f) 10 wt % Re/Fe_2O_3 (Fe_2O_3 prepared by the decomposition of NH_4ReO_4 at 673 K), (g) 10 wt % Re/γ-Fe_2O_3, (h) commercially available α-Fe_2O_3, (i) commercially available γ-Fe_2O_3.

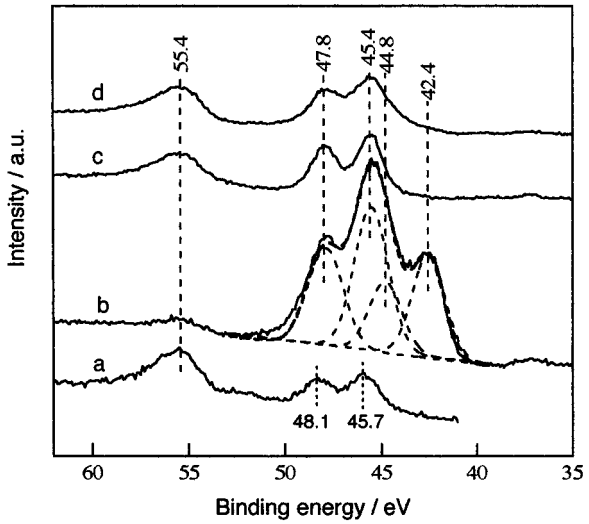

Figure 6. Re 4f and Fe 3p XPS spectra for iron-oxide supported ReO_x catalysts with 10 wt % Re: (a) NH_4ReO_4/α-Fe_2O_3 catalyst, (b) Re/α-Fe_2O_3 catalyst, (c) Re/γ-Fe_2O_3 catalyst, (d) Re/Fe_2O_3 catalyst.

crystallization to ReO_2. In the case of the 10 wt % Re/α-Fe_2O_3 catalyst with a low surface area (3 m^2 g^{-1}), small peaks due to ReO_2 were observed, as shown in Figure 5c. The state of the rhenium oxides did not change after catalytic methanol oxidation at 513 K for 2 h, as shown in Figure 5d.

Figure 6 shows the Re 4f and Fe 3p XPS spectra for Re/α-Fe_2O_3, Re/γ-Fe_2O_3, and Re/Fe_2O_3 with 10 wt % Re. For comparison, the XPS spectrum for as-prepared NH_4ReO_4/α-Fe_2O_3 is also shown in Figure 6. The XPS spectra for the Re/α-Fe_2O_3 catalyst showed a peak at 42.4 eV, which is assigned to the Re $4f_{7/2}$ level for Re^{4+} species, and a peak at 47.8 eV, which is assigned to the Re $4f_{5/2}$ level for the Re^{6-7+} species. The most intense peak around 45 eV is then considered as the sum of the Re $4f_{7/2}$ peak for the Re^{6-7+} species and the Re $4f_{5/2}$ peak for the Re^{4+} species. The peak around 45 eV was deconvoluted into two peaks at 45.4 and 44.8 eV for Re^{6-7+}

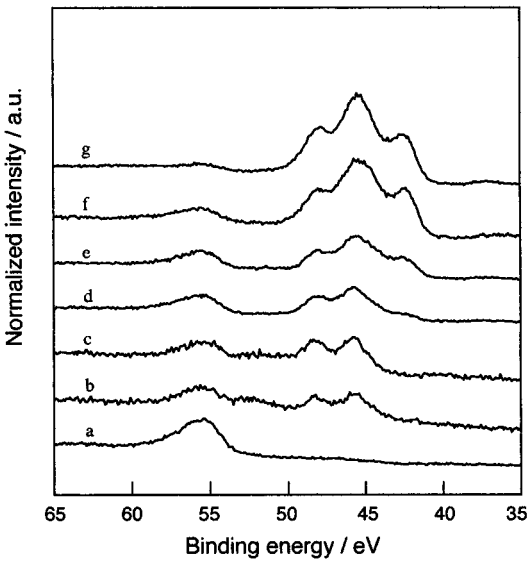

Figure 7. Re 4f and Fe 3p XPS spectra for the Re/α-Fe_2O_3 catalysts. Re loading (wt %): (a) 0.0, (b) 0.5, (c) 1.0, (d) 2.0, (e) 3.0, (f) 6.0, (g) 10.0.

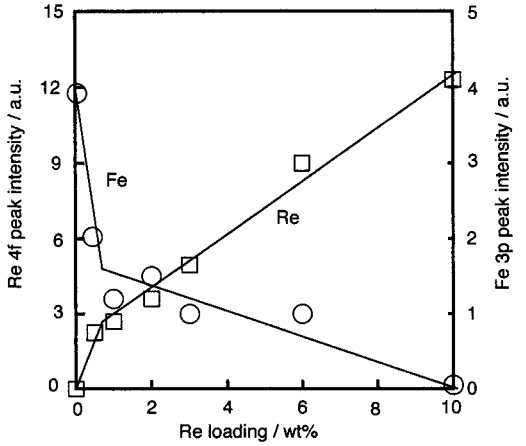

Figure 8. Dependencies of the intensities of Re 4f and Fe 3p XPS peaks normalized to the intensity of O 1s peaks on Re loading in the Re/α-Fe_2O_3 catalysts.

$4f_{7/2}$ and Re^{4+} $4f_{5/2}$, respectively. The binding energy of 45.4 eV is lower by 1.0−1.4 eV than that reported for Re_2O_7 (Re^{7+}) but higher by 1.0−1.2 eV than that for ReO_3 (Re^{6+}).[33,34] The NH_4ReO_4/α-Fe_2O_3 catalyst with Re^{7+} exhibited the binding energies of 48.1 and 45.7 eV for Re $4f_{5/2}$ and $4f_{7/2}$, respectively (Figure 6a). In contrast, the Re/γ-Fe_2O_3 and Re/Fe_2O_3 catalysts showed no Re^{4+} XPS peaks, and only Re^{6-7+} species were present at the catalyst surfaces (Figure 6c and d). Fe 2p and 3p bands appeared at binding energies of 711.0 and 55.4 eV, respectively, which are the values typical of Fe^{3+} for α-Fe_2O_3.

Figure 7 shows the Re 4f and Fe 3p XPS spectra for the Re/α-Fe_2O_3 catalysts with different Re loadings. The catalysts with Re loadings of 0.5 and 1.0 wt % contained only Re^{6-7+} species. For Re loadings of 2.0−10.0 wt %, Re^{4+} peaks appeared in addition to the Re^{6-7+} peaks. The Fe 3p binding energies were almost the same as those for α-Fe_2O_3. The XPS intensities of the Re (all $4f_{5/2}$ and $4f_{7/2}$) and Fe 3p peaks are plotted against the Re loading in Figure 8. The XPS intensities are normalized by the O (1s) intensity in each catalyst. There are clear breaks at 0.7−0.8 wt % in both plots, although the data are somewhat scattered. The features of Figure 8 can be explained by the Stranski−Krastanov growth mode for rhenium oxides on α-Fe_2O_3.[35]

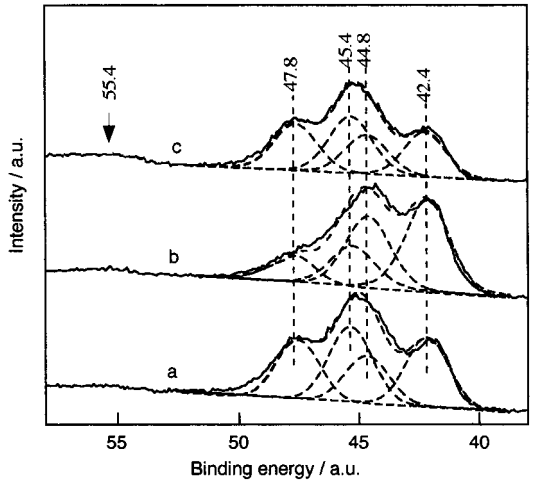

Figure 9. Re 4f and Fe 3p XPS spectra for the 10 wt % ReO_x/Fe_2O_3 catalysts: (a) after pretreatment at 673 K for 6 h in He, (b) after 10 methnaol pulses (He/MeOH) at 513 K, and (c) after catalytic methanol oxidation at 513 K for 2 h.

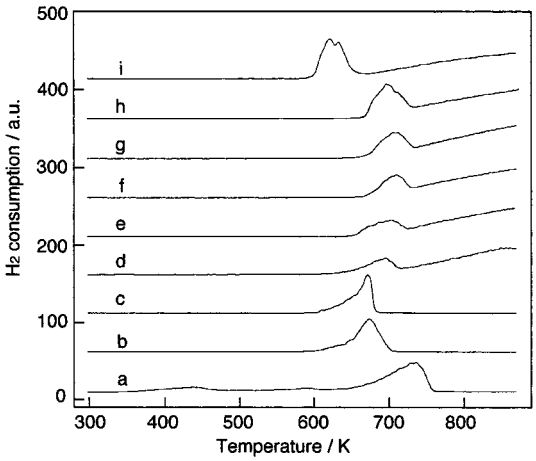

Figure 10. TPR profiles for (a) commercially available ReO_2, (b) commercially available ReO_3, (c) commercially available NH_4ReO_4, (d) commercially available α-Fe_2O_3, (e) 1.0 wt % Re/α-Fe_2O_3 catalyst, (f) 2.0 wt % Re/α-Fe_2O_3 catalyst, (g) 6.0 wt % Re/α-Fe_2O_3 catalyst, (h) 10.0 wt % Re/α-Fe_2O_3 catalyst, (i) 10.0 wt % NH_4ReO_4/α-Fe_2O_3.

Figure 9 shows the Re 4f XPS spectra for the 10 wt % Re/α-Fe_2O_3 catalysts (a) after treatment at 673 K for 6 h in He, (b) after the 10 methanol pulses at 513 K, and (c) after catalytic methanol oxidation at 513 K for 2 h. After the 10 methanol pulses at 513 K, the Re 4f XPS spectrum exhibited a significant decrease in the peak intensity for the Re^{6-7+} species, whereas the intensity of the Re^{4+} peaks increased. After the catalytic methanol oxidation at 513 K, the XPS spectrum had features similar to those in the spectrum for the fresh catalyst.

3.5. H_2 TPR and Pyridine TPD and FTIR Spectroscopy. To examine the redox and acidic properties of the Re/α-Fe_2O_3 catalysts (as selective methanol conversion to methylal involves both oxidation and dehydration steps), H_2 TPR and pyridine TPD and FTIR data were collected for the catalysts and reference compounds. The TPR profiles for ReO_2, ReO_3, NH_4ReO_4, α-Fe_2O_3, 10 wt % NH_4ReO_4/α-Fe_2O_3, and Re/α-Fe_2O_3 catalysts with different Re loadings are shown in Figure 10. The TPR peak for ReO_2 was as high as 730 K, whereas the TPR peak for ReO_3 was observed at 675 K, which was slightly higher than that for NH_4ReO_4. Reduction of α-Fe_2O_3 occurred around 700 K, which is ascribed to the reduction of Fe_2O_3 to Fe_3O_4.[36] The 10 wt % NH_4ReO_4/α-Fe_2O_3 catalyst showed TPR

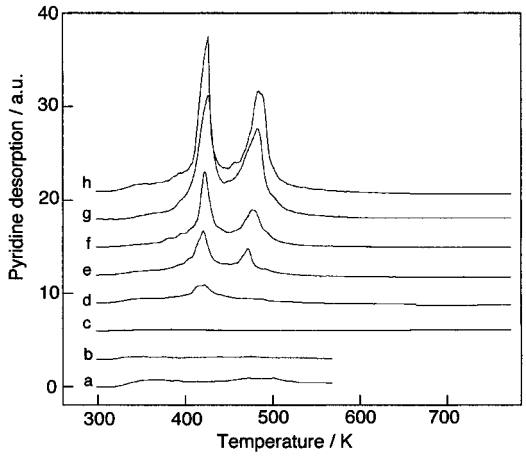

Figure 11. Pyridine TPD spectra for (a) commercially available ReO_2, (b) commercially available ReO_3, (c) commercially available α-Fe_2O_3, (d) 1.0 wt % Re/α-Fe_2O_3 catalyst, (e) 2.0 wt % Re/α-Fe_2O_3 catalyst, (f) 3.0 wt % Re/α-Fe_2O_3 catalyst, (g) 6.0 wt % Re/α-Fe_2O_3 catalyst, (h) 10.0 wt % Re/α-Fe_2O_3 catalyst. ReO_2 and ReO_3 were pretreated at 573 K for 1 h in He, whereas the other catalysts were pretreated at 673 K for 1 h in He.

TABLE 2: Number of Desorbed Pyridine Molecules[a] in the Low- and High-Temperature Peaks in the TPD Spectra for the Re/α-Fe_2O_3 Catalysts with Different Re Loadings

Re loading (wt %) (μmol/mg)	0.0	1.0	2.0	3.0	6.0	10.0
peak α	0	0.0148	0.0503	0.0575	0.1052	0.0919
peak β	0	0	0.0239	0.0566	0.1381	0.1408

[a] Number of Lewis acid sites.

peaks at 620−630 K, which is lower than the NH_4ReO_4 TPR peak because of dispersion of NH_4ReO_4 on the support. For the Re/α-Fe_2O_3 catalysts TPR peaks at 713 and 696 K developed with increasing Re loading. The TPR peak features for the 1 wt % Re/α-Fe_2O_3 catalyst were different from those for the other Re/α-Fe_2O_3 catalysts. Further increase of Re loading to 10 wt % gave a shoulder peak at 680 K in addition to the peaks at 696 and 713 K (Figure 10h). The TPR spectrum for the 10 wt % ReO_x/γ-Fe_2O_3 catalyst exhibited two reduction peaks at 693 and 742 K. γ-Fe_2O_3 had a reduction peak at 719 K. The separation of the two peaks was more definite than for Fe/α-Fe_2O_3, but the origins of the TPR peaks should be similar.

Figure 11 shows pyridine TPD spectra for Re/α-Fe_2O_3 catalysts with different Re loadings, ReO_2, ReO_3, and α-Fe_2O_3. No significant pyridine adsorption occurred on α-Fe_2O_3, ReO_2, and ReO_3. However, two desorption peaks at 417−426 and 470−479 K were observed for the Re/α-Fe_2O_3 catalysts with 1.0−10.0 wt % Re loadings. The amounts of pyridine desorbed in the two peaks are listed in Table 2. The amounts increased with increasing Re loading up to 6 wt % Re, where it was nearly saturated. Two distinct desorption peaks at 450 and 500 K were also observed for Re/γ-Fe_2O_3, whereas the desorption of pyridine from γ-Fe_2O_3 alone was negligible. There was no significant difference in the TPD features for the α-Fe_2O_3- and γ-Fe_2O_3-supported samples.

The nature of the acidic sites was examined by FTIR spectroscopy for adsorbed pyridine on 6.0 wt % ReO_x/α-Fe_2O_3. The FTIR spectrum exhibited weak peaks at 1450, 1494, and 1588 cm^{-1}, which are assigned to pyridine coordinated to Lewis acidic sites. There was no peak due to pyridine adsorbed on Brönsted acidic sites. Under identical conditions, almost no desorption peak was observed with the α-Fe_2O_3 support alone.

4. Discussion

4.1. Catalytic Properties of Supported Rhenium Oxides for the Selective Oxidation of Methanol to Methylal. Many catalysts have been screened to improve the performance in the selective methanol conversion to methylal, but no supported rhenium oxides have been reported to date.[31] V/TiO_2,[24] V−Mo−O,[25] PMoH-5.75/SiO_2,[26,27] Mo/MCM-41,[28] and others[29,30] have been claimed to be active for catalytic methylal synthesis from methanol. The selectivities toward methylal on V/TiO_2 and PMoH-5.75/SiO_2 were as low as 40−56%. The Mo/MCM-41 catalyst showed a selectivity of 76.2% at a low conversion of 0.7% at 543 K, but rapid deactivation was a serious problem because of the a significant leaching of Mo species from MCM-41. Recently, we found that crystalline $SbRe_2O_6$ exhibited excellent performances in the catalytic selective oxidation of methanol to methylal.[22,23] A high selectivity of 92.5% to methylal at 6.5% conversion at 573 K was achieved on the new crystalline catalyst, where the high performance of $SbRe_2O_6$ was ascribed to the rhenium oxide species stabilized by specific connections with to antimony oxides at the crystal surface. Extending our knowledge about and achievements with the crystalline catalyst, we have found a new catalytic property of supported rhenium oxides that provides a promising one-stage process for catalytic methylal synthesis from methanol that is preferable economically and environmentally to the two-stage industrial processes involving methanol oxidation to formaldehyde on silver or ferric molybdate catalysts and dehydrative condensation (acetalization) of the formaldehyde with methanol using sulfuric acid as a catalyst.[31] The selectivities of Re/α-Fe_2O_3, Re/γ-Fe_2O_3, and Re/V_2O_5 were 90.5−93.7% at conversions of 15.5−48.4% at 513 K, as shown in Table 1. The selectivities of these catalysts are similar to that of $SbRe_2O_3$, but their catalytic activities are much larger than the activity of $SbRe_2O_6$. It is to be noted that α-Fe_2O_3 is inactive for methylal synthesis and V_2O_5 is active only for formaldehyde formation. Rhenium oxide species supported on the oxide supports showed remarkable performances for catalytic methylal synthesis by one-stage methanol conversion.

The plots of the reaction rate versus the surface area in Figure 1, which correspond to the efficiencies per 1 wt % Re quantity of the catalysts, indicate that the supported ReO_x catalysts employed in this study can be classified into four groups from the viewpoint of the reactivity of the ReO_x species. The Re/TiO_2 (rutile) catalyst shows a high activity even though the surface area is as small as 5 m^2 g^{-1}, whereas the Re/SiO_2 catalyst, which has a relatively high surface area of 36 m^2 g^{-1}, shows a low activity. The Re/TiO_2 (anatase) catalyst with the largest surface area among the employed catalysts shows the highest activity per gram of Re, but the reactivity of the ReO_x species on TiO_2 (anatase) is similar to the reactivities of the Re/α-Al_2O_3 and Re/MoO_3 catalysts, which have intermediate selectivity values. The Re/α-Fe_2O_3, Re/γ-Fe_2O_3, Re/V_2O_5, and Re/ZrO_2 catalysts are grouped according to the similar reactivities per unit surface area of the rhenium oxide species. This group shows high selectivities for the catalytic methylal synthesis. The classification can be justified by the plots of selectivity versus conversion per unit surface area in Figure 1. The selectivity increased with increasing conversion, passed through a maximum, and then gradually decreased with further increasing conversion. The results demonstrate that the medium activity (conversion per unit surface area) leads to the high selectivity often observed in many catalytic processes. The Re/α-Fe_2O_3, Re/γ-Fe_2O_3, Re/V_2O_5, and Re/ZrO_2 catalysts exhibited good performances for the catalytic selective oxidation of

methanol to methylal: 90.5% selectivity at 15.5% conversion, 91.0% selectivity at 48.4% conversion, 93.7% selectivity at 21.5% conversion, and 89.4% selectivity at 35.8% conversion, respectively, as shown in Table 1.

The conversion increased with reaction temperature, whereas the selectivity to methylal passed through a maximum at 513 K andt hen decreased with increasing temperature, as shown in Figure 3. However, the selectivity to methylal (product) + formaldehyde (intermediate) maintained high values of 92.5% at 15.5% conversion (513 K), 92.5% at 21.5% conversion (533 K), and 90.0% at 28.8% conversion (553 K). The fact that the production of undesirable products such as dimethyl ether, CO, and CO_2 does not increase significantly with reaction temperature also provides evidence that the supported rhenium oxides are promising catalysts for selective methanol conversion to methylal. Hereinafter, the surface states of Re/α-Fe_2O_3 and Re/γ-Fe_2O_3 as the representative catalysts are discussed in relation to the active Re species for catalytic methylal synthesis.

4.2. Surface States of Fe_2O_3-Supported Re Catalysts. A monolayer coverage of ReO_x species on α-Fe_2O_3 surface is calculated to be about 0.7 wt % Re by assuming the cross section of a ReO_3 unit (selective bulk) to be 1.39×10^{-19} m^2. In the plots of the Re 4f and Fe 3p XPS peak intensities versus Re loading in Figure 8 there were definite breaks at 0.7−0.8 wt % Re loading, followed by gently sloping straight lines, although the data were somewhat scattered. The break feature in the XPS plots of Figure 8 can be explained by the Stranski−Ktastanov growth mode,[35] in which ReO_x species are dispersed up to a monolayer coverage at the break and then three-dimensional (3D) rhenium oxide species are formed on the ReO_x monolayer.

Both the catalytic conversion and selectivity increased linearly with increasing Re loading in the range 0−1 wt % and further increased up to 3 wt % Re loading, which is about 4 times larger than monolayer coverage (Figure 2). Thus, the monolayer ReO_x species are active for the selective methanol conversion to methylal, but the 3D rhenium oxide species on the monolayer species are more active than the monolayer species. Above 3 wt % Re, neither conversion nor selectivity continued to increase, as shown in Figure 2. The active rhenium oxides at the catalyst surface were saturated at 3 wt %. On the other hand, the XPS Re 4f signals further increased with an increase in Re loading above 3 wt %. The escape depth of the photoelectrons for Re 4f levels in the XPS spectra is 1.5 nm, which means that the XPS signals provide information on rhenium oxides in not only the catalytically active outermost surface layer but also several surface layers. The XPS spectra in Figure 7 reveal that Re^{4+} species appear at 2−3 wt % Re loadings, but they are less important than the Re^{6-7+} species in the catalytic performance, as no Re^{4+} species are observed for the 10 wt % Re/γ-Fe_2O_3 catalyst with 91.0% selectivity (Figure 6). Above 3 wt % Re loading, the conversion and selectivity decreased slightly (Figure 2). The decrease might be due to the increase of Re^{4+} species in the Re/α-Fe_2O_3 catalysts with 6−10 wt % Re, as shown in Figure 7. ReO_2 crystallites were observed for the 10 wt % Re/α-Fe_2O_3 catalyst (Figure 5c). ReO_2 crystallites are also active for methylal synthesis, but their selectivity is much smaller than that for ReO_3 (Table 1).

To clarify the oxidation state of the active rhenium oxide species, we measured XPS spectra for the Re/α-Fe_2O_3 and Re/γ-Fe_2O_3 catalysts (Figures 6 and 7). The binding energies of 47.8 eV (Re $4f_{5/2}$) and 45.4 eV (Re $4f_{7/2}$) observed with the 3−10 wt % Re/α-Fe_2O_3 catalysts in Figure 7 were lower by 1.0−1.4 eV than those for Re_2O_7 (Re^{7+}) but higher by 1.0−1.2 eV than those for ReO_3 (Re^{6+}).[33,34] The values for the catalysts

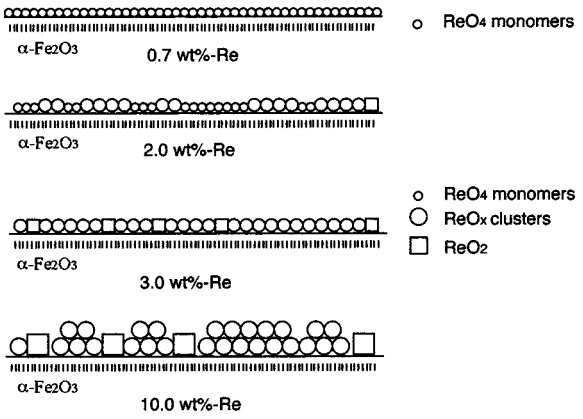

Figure 12. Surface models for the Re/α-Fe_2O_3 catalysts with Re loadings of 0.7, 2.0, 3.0, and 10 wt %. Small circles, ReO_4 monomers; large circles, ReO_x clusters (probably Re−Fe−O phase); squares, ReO_2.

are intermediate between those for bulk Re_2O_7 and bulk ReO_3. However, the 0.5−1 wt % Re/α-Fe_2O_3 catalysts with rhenium oxides in the monolayer show 48.2 and 45.7 eV for Re $4f_{5/2}$ and $4f_{7/2}$, respectively. The values are almost the same as the values (48.1 and 45.7 eV) obtained for NH_4ReO_4 with tetrahedral Re^{7+} dispersed on α-Fe_2O_3 (Figure 6). The XAFS study on a monolayer Re/γ-Fe_2O_3 catalyst has revealed that the rhenium oxides on γ-Fe_2O_3 were dispersed as [ReO_4] species with a tetrahedral symmetry.[37] The preliminary EXAFS analysis for the Re/γ-Fe_2O_3 catalysts also revealed the presence of Re−O−Fe bonding at high Re loadings above a monolayer.[37] Thus, it is suggested that the Re species are stabilized by making Re−O−Fe bonds. We assume the growth of a 3D Re−Fe−O mixed-oxide phase following [ReO_4] monolayer formation. The active 3D rhenium oxides are saturated at four-layer coverage on average, indicating that the rhenium oxide clusters are small. The number of rhenium oxide clusters increases with increasing Re loading in the range 0.7−3.0 wt %. As a consequence, the surface states illustrated in Figure 12 are proposed for the Re/α-Fe_2O_3 catalysts.

In the pyridine TPD spectra of the 1.0 wt % Re/α-Fe_2O_3 catalyst with a Re loading of about 1.4 monolayers in Figure 11, only one peak at 417 K is observed. According to the above discussion, the peak is assigned to mainly the tetrahedral [$Re^{7+}O_4$] species dispersed in the monolayer on the α-Fe_2O_3 surface. Hence, the acidity of the dispersed Re^{7+} species is weak. At Re loadings larger than 1.0 wt %, there are two peaks at 417−426 and 470−479 K (Figure 12 and Table 2). The 2 wt % Re/α-Fe_2O_3 catalyst shows two TPD peaks at 420 and 470 K. The TPD data also indicate the formation of different Re species from the tetrahedral [ReO_4] species in the samples with larger-than-monolayer Re loadings. The intensities of both low- and high-temperature TPD peaks increased with increasing Re loading from 3 to 6 wt % and nearly saturated or decreased slightly at 10 wt % (Table 2). The conversion and selectivity for catalytic methylal synthesis were saturated at 3 wt % Re loading, as shown in Figure 2. There is no relationship between the results of Figures 2 and 11, and hence, the acidity of the surface is not a decisive factor in the catalytic performance.

The TPR spectra also increased in intensity with increasing Re loading (Figure 10). The absolute quantities of hydrogen molecules consumed in the TPR spectra in Figures 10 and 11 could not be determined exactly under the present experimental conditions given certain experimental errors. However, we can discuss the relative change in different Re loadings. The TPR data reflect the redox properties of at least a few surface layers. The dependency of the catalytic performance on the Re loading

(Figure 2) is different from that of the TPR peak intensity (Figure 10), which indicates that the catalytic performance can be ascribed to the redox property of the outermost surface layer of rhenium oxide clusters with suitable acidities. In fact, all of the Re^{6-7+} species were not reduced by methanol exposure at 513 K, as shown in Figure 9. In the pulse experiments on the 10.0 wt % Re/a-Fe_2O_3 catalyst at 513 K using a mixture of 96.0/4.0 (mol %) He/MeOH in the absence of O_2 (Figure 4), methylal formation decreased with an increase in the number of the pulses, and after the fifth pulse, no methylal was produced. It is evident that the lattice oxygen atoms of the rhenium oxide clusters work as active oxygen species for the selective oxidation of methanol. After 10 methanol pulses at 513 K, the intensities of the XPS peaks at 47.8 and 45.4 eV decreased, whereas the Re^{4+} peak intensities increased (Figure 9b). The consumed lattice oxygen atoms were replenished by gaseous O_2, as verified by the XPS spectrum of Figure 9c. The results indicate that the redox capability of the rhenium oxide species, $Re^{6-7+} \leftrightarrows Re^{4+}$, is responsible for the selective oxidation of methanol.

In methanol conversion to methylal, the first reaction step has been demonstrated to be the formation of methoxy species.[38,39] Further transformation of the methoxy species depends on the redox and acid−base properties of the active rhenium oxides. Desorption of formaldehyde produced by dehydrogenation of the methoxy species is favored on weak acid sites. If the active sites are strongly acidic, the residence time of the formaldehyde becomes long enough for dioxymethylene species to be formed,[39] and the dioxymethylene species can then react with neighboring methoxy species and/or adsorbed methanol to form methylal.[40] If both athe cidic and basic sites are too strong, the dioxymethylene species are oxidized to formates, which also react with methanol to form methyl formate or are further oxidized to carbon dioxides.[39] If strong acid sites and very weak basic sites are present at catalyst surfaces, only dimethyl ether is formed.[41] The present results indicate that the Re/Fe_2O_3 catalysts can fit the requirements for both "redox" and "acid−base" catalyses for selective methanol oxidation to methylal. The bifunctional catalysis of moderate redox and acidic properties at the Re/Fe_2O_3 catalyst surface might benefit from the $Re^{6-7+}O_x$ clusters (probably a Re−Fe−O phase) grown following the formation of the $[Re^{7+}O_4]$ monolayer chemically bound to the Fe_2O_3 surface.

5. Conclusion

(1) α-Fe_2O_3-, γ-Fe_2O_3-, and V_2O_5-supported ReO_x catalysts exhibited high activities and selectivities for the catalytic selective oxidation of methanol to methylal, with 90−94% selectivities at 15−49% conversions at 513 K.

(2) The highest reaction rate, in units of moles per hour per mole of Re, on the Re/α-Fe_2O_3 catalysts was achieved in the range of Re loadings of 1−3 wt %.

(3) Interactions between the rhenium oxides and the Fe_2O_3 supports (probably Re−O−Fe bonding) generated by the treatment of supported NH_4ReO_4 precursor at 673 K in He caused stabilization of dispersed tetrahedral $Re^{7+}O_4$ species (≤0.7 wt % Re) on the α-Fe_2O_3 surface and prevented the Re^{7+} species from being reduced to $Re^{4+}O_2$.

(4) Active $Re^{6-7+}O_x$ clusters (probably Re−Fe−O phase) were formed on α-Fe_2O_3 at Re loadings ≥1 wt % after the formation of a $[Re^{7+}O_4]$ monolayer.

(5) On α-Fe_2O_3, $Re^{4+}O_2$ species were formed at Re loadings of ≥ 3 wt %, and ReO_2 crystallites were also formed at a Re loading of 10 wt %.

(6) On γ-Fe_2O_3, no Fe^{4+} oxides were observed for the fresh 10 wt % Re catalyst.

(7) The ReO_x species supported on the Fe_2O_3 surfaces showed a TPR profile different from those for NH_4ReO_4, ReO_3, and ReO_2.

(8) Lattice oxygen atoms of the ReO_x species were active for the catalytic methylal synthesis, and the consumed oxygen atoms are replenished by O_2 under the reaction conditions used.

(9) ReO_2, ReO_3, α-Fe_2O_3, and γ-Fe_2O_3 showed negligible pyridine adsorption, whereas the active ReO_x/α-Fe_2O_3 and ReO_x/γ-Fe_2O_3 catalysts showed two pyridine TPD peaks at 420−450 and 470−500 K.

(10) The redox capability of rhenium oxides between Re^{6-7+} and Re^{4+} on the supports might be responsible for the selective oxidation of methanol to formaldehyde, and the appropriate acidity of rhenium oxides might also be necessary for the acetalization of formaldehyde with methanol to form methylal.

Acknowledgment. This work was supported by Core Research for Evolutional Science and Technology (CREST) of Japan Science and Technology Corporation (JST) and partially supported by the Natural Science Foundation of China (NSFC).

References and Notes

(1) Bastide, B.; Enjalbert, R.; Fuess, H.; Galy, J. *Solid State Chem.* **2000**, *2*, 545.
(2) Watanebe, H.; Imoto, H.; Tanaka, H. *J. Solid State Chem.* **1998**, *138*, 245.
(3) Butz, A.; Miehe, G.; Paulus, H.; Strauss, P.; Fuess, H. *J. Solid State Chem.* **1998**, *138*, 232.
(4) Liu, H.; Gaigneaux, E. C.; Imoto, H.; Shido, T.; Iwasawa, Y. *J. Phys. Chem.* **2000**, *104*, 2033.
(5) Liu, H.; Shido, T.; Iwasawa, Y. *Chem. Commun.* **2000**, 1881.
(6) Moulijn, J. A.; Mol, J. C. *J. Mol. Catal.* **1988**, *46*, 1. Mol, J. C.; Moulijn, J. A. In *Advance in Catalysis*; Eley, D. D., Pines, H., Weisz, P. B., Eds.; Academic Press: New York, 1975; Vol. 24, p 131.
(7) Olsthoorn, A. A.; Boelhouwer, C. *J. Catal.* **1976**, *44*, 207.
(8) Augustine, S. M.; Sachtler, W. M. H. *J. Catal.* **1989**, *116*, 184.
(9) Pecoraro, T. A.; Chianelli, R. R. *J. Catal.* **1981**, *67*, 430.
(10) Thomas, R.; Van Oers, E. M.; De Beer, V. H. J.; Medema, J.; Moulijn, J. A. *J. Catal.* **1982**, *76*, 241.
(11) Albonetti, S.; Cavani, F.; Trifiro, F. *Catal. Rev.−Sci. & Eng.* **1996**, *38*, 413.
(12) Warwel, S.; Rüsch, M.; Sojka, M. *J. Chem. Soc., Chem. Commun.* **1991**, 1578.
(13) Sheldon, R. A.; Kochi, J. K. *Metal-Catalyzed Oxidation of Organic Compounds*; Academic Press: New York, 1981.
(14) *Organic Syntheses by Oxidation with Metal Compounds*; Mijis, W. J., de Jonge, C. R. H. J., Eds.; Plenum Press: New York, 1986.
(15) Jacobsen, E. N.; Marcó, I.; Mungall, W. S.; Schröder, G.; Sharpless, K. B. *J. Am. Chem. Soc.* **1988**, *110*, 1968.
(16) Herrmann, W. A.; Eder, S. J.; Scherer, W. *Angew. Chem., Int. Ed. Engl.* **1992**, *31*, 1345.
(17) Herrmann, W. A. *Angew. Chem., Int. Ed. Engl.* **1988**, *27*, 1297.
(18) Sundermeyer, J. *Angew. Chem.* **1993**, *105*, 1195.
(19) Herrman, W. A.; Fischer, R. W.; Rauch, M. U.; Scherer, W. *J. Mol. Catal.* **1994**, *86*, 243.
(20) Espenson, J. H. *Chem. Commun.* **1999**, 479.
(21) Owens, G. S.; Arias, J.; Abu-Omar, M. M. *Catal. Today* **2000**, *55*, 317.
(22) Yuan, Y.; Liu, H.; Imoto, H.; Shido, T.; Iwasawa, Y. *Chem. Lett.* **2000**, 674.
(23) Yuan, Y.; Liu, H.; Imoto, H.; Shido, T.; Iwasawa, Y. *J. Catal.* **2000**, *195*, 51.
(24) Tatibouët, J. M. *Appl. Catal. A: Gen.* **1997**, *148*, 213.
(25) Tatibouët, J. M.; Germain, J. E. *Bull. Soc. Chim. Fr.* **1980**, *9−10*, 343.
(26) Fournier, M.; Aouissi, A.; Rocchiccioli-Deltchff, C. *J. Chem. Soc., Chem. Commun.* **1994**, 307.
(27) Rocchiccioli-Deltcheff, C.; Aoussi, A.; Launary, S.; Fournier, M. *J. Mol. Catal. A: Chem.* **1996**, *114*, 331.
(28) Shannon, I. J.; Maschmeyer, T.; Oldroyd, R. D.; Sankar, G.; Thomas, J. M.; Pernot, H.; Baalikdjian, J. P.; Che, M. *J. Chem. Soc., Faraday Trans.* **1998**, *94*, 1495.
(29) Tatibouët, J. M.; Germain, J. E.; Volta, J. C. *J. Catal.* **1983**, *82*, 240.

(30) For example, see: Otsuka, K.; Yamanaka, I. *Appl. Catal*. **1986**, *26*, 401.
(31) Yuan, Y.; Shido, T.; Iwasawa, Y. *Chem. Commun.* **2000**, 1421.
(32) Abakumov, A. M.; Shpanchenko, R. V.; Antipov, E. V. *Z. Anorg. Allg. Chem*. **1998**, *624*, 750.
(33) Shpiro, E. S.; Avaev, V. I.; Antoshin, G. V.; Ryashentseva, M. A.; Minachev, K. M. *J. Catal.* **1978**, *44*, 4022.
(34) Cimino, A.; De Angelis, B. A.; Gazzoli, D.; Valigi, M. *Z. Anorg. Allg. Chem*. **1980**, *460*, 86.
(35) Shido, T.; Okita, G.; Asakura, K.; Iwasawa, Y. *J. Phys. Chem.* **2000**, *104*, 12263.
(36) Basiska, A.; Klimkiewicz, R.; Domka, F. *Appl. Catal. A: Gen.* **2001**, *207*, 287.
(37) Nakagawa, F.; Sasaki, T.; Shido, T.; Iwasawa, Y., to be published.
(38) Chung, J. S.; Miranda, R.; Bennertt, C. O. *J. Catal*. **1988**, *114*, 354.
(39) Busca, G. *Catal. Today* **1996**, *27*, 457.
(40) Yang, T. J.; Lunsford, J. H. *J. Catal*. **1987**, *103*, 55.
(41) Chauvin, C.; Saussey, J.; Lavalley, J. C.; Idriss, H.; Hindermann, J. P.; Kienneman, A.; Chaumette, P.; Courty, P. *J. Catal*. **1990**, *121*, 56.